Available online at www.sciencedirect.com
SCIENCE DIRECT®
Journal of Solid State Chemistry 177 (2004) 4465–4474
JOURNAL OF SOLID STATE CHEMISTRY
www.elsevier.com/locate/jssc

$LiLa_6I_{12}Os$, a substitutional derivative of rhombohedral $La(La_6I_{12}Os)$

Elizabeth A. Jensen, John D. Corbett*

Department of Chemistry, Iowa State University, Room 353, Spedding Hall, Ames, IA 50011-3020, USA

Received 16 April 2004; received in revised form 2 August 2004; accepted 9 August 2004

Abstract

The series of quaternary rare-earth-metal halide cluster compounds $ALa_6I_{12}Z$ with transition metal interstitials Z and alkali or alkaline-earth metal cations A has been expanded to include $A = Li$. The compounds synthesized by high-temperature solid-state techniques for $Z = Os$, Ir, Pt, Ru are isotypic with rhombohedral $R_7X_{12}Z$ ($R\bar{3}$, $Z = 3$). The refined single X-ray crystal structure of $(Li_{0.967}La_{0.033})La_6I_{12}Os$ is reported, along with supportive results from a Rietveld analysis of neutron powder diffraction from a different sample, ^7Li MAS-NMR, and electronic resistivity and magnetic susceptibility measurements. The samples show continuous $Li_{1-x}La_x$ cation compositions and are generally semiconductors, but their complex paramagnetic properties are not those of simple spin-only systems.

Keywords: Rhombohedral; $LiLa_6I_{12}Os$; Semiconductors

1. Introduction

Reduced rare-earth-metal (R) halides form only three structures that contain isolated $R_6X_{12}(Z)$-type clusters in which $X = Cl$, Br, I and Z is a centered transition metal or other interstitial atom, namely with $R_7X_{12}Z$, $R_6X_{10}Z$, and $R_{12}X_{17}Z$ stoichiometries. Other cluster halides contain condensed bioctahedral units, oligomers of four octahedra, or infinite chains or layers of octahedra, all of which are centered. The variety of bridging halide modes possible leads to a vast array of compositions and structures [1–3], and these can be further extended through the inclusion of cations of the more active metals.

The rhombohedral ($R\bar{3}$) $R_7X_{12}Z$ structure is the most versatile example, known for $R = Sc$, Y, and most of La–Lu with the three heavier halides, although the bromides have been considerably less well studied. These compounds accept a great variety of interstitial elements Z, including most of the transition metals in groups 7–11 as well as main group elements (B, C, N, Si, etc.). The structure, Fig. 1, consists of R_6 trigonal antiprismatic ($\bar{3}$) clusters that are only slightly distorted from ideal octahedra, and have Z bound in their centers. All twelve edges of each metal cluster are bridged by one of two crystallographically distinct X. Six inner $X1$ atoms bridge the R–R edges of the basal faces (as X^i). The other six edges around the cluster waist are bridged by bifunctional $X2$ atoms that also form exo bonds to metal vertices of adjacent clusters (X^{i-a}). Reciprocally, the metal atom vertices of each cluster are terminally bonded to $X2$ atoms which bridge R–R waist edges of neighboring clusters as well (X^{a-i}). The seventh R atom (crystallographically $R2$) is located on a $\bar{3}$ site halfway between R_6Z clusters along c so that it is surrounded by six trigonal antiprismatic $X1$ atoms from the clusters above and below. A more detailed formulation of $R_7X_{12}Z$ is thus $R^{+3}[R_6(Z)(X1^i)_6(X2^{i-a})_{6/2}(X2^{a-i})_{6/2}]^{-3}$ [4,5].

Experience with other structures and compositions has shown that introduction of alkali or alkaline-earth metal cations and the corresponding electrons or halide anions may produce new compounds with more reduced or more open structural frameworks of the metal–halide

*Corresponding author. Fax: +1-515-294-5718.
E-mail address: jcorbett@iastate.edu (J.D. Corbett).

0022-4596/$ - see front matter © 2004 Elsevier Inc. All rights reserved.
doi:10.1016/j.jssc.2004.08.031

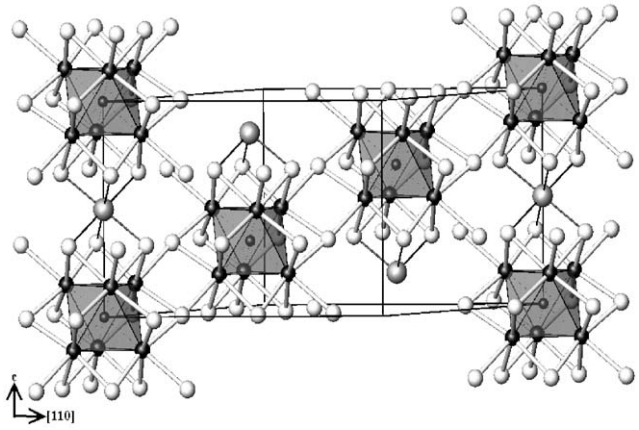

Fig. 1. The structure of L0i$La_6I_{12}Os$, showing a [110] section of several chains of $La_6I_{12}Os$ clusters. Small black, large black, large gray, and white spheres represent Os, La, Li and I, respectively. In the parent compounds, $La_7I_{12}Os$, the Li position is occupied by La2.

clusters. The cations mainly fulfill charge requirements, as in the compounds $AR_6I_{10}Z$ (A = K, Cs; R = La, Pr; Z = Mn, Fe, Os) [6], $Cs_4R_6I_{13}Z$ (R = Ce, Pr; Z = Co, Os) [7], and $Cs_2La_{10}I_{17}Co_2$ [8]. Earlier attempts to substitute the $R2$ position in $R_7X_{12}Z$ structures by Ca resulted in only partial substitution in $(Ca_{0.65}Pr_{0.35})Pr_6I_{12}Co$, $(Ca_{1-y}Gd_y)Gd_6I_{12}Fe$, and $(Ca_{1-z}Gd_z)Gd_6I_{12}Co$ products [5]. Another investigation yielded $CsEr_6I_{12}C$ with a comparable stoichiometry, but with a different cation position and differently interconnected clusters [9]. A complete substitution of the isolated $R2$ atom in the $R_7X_{12}Z$ structure type was first discovered in the isotypic $NaLa_6I_{12}Os$ [10] during attempts to synthesize analogues of $K_4La_6I_{14}Os$ [11]. We have recently reported a corresponding series of new $ALa_6I_{12}Z$ phases with A = Na, Mg, Ca, Sr and some of their electrical and magnetic properties [12,13]. The following details the particular problems with and properties of the remaining $LiLa_6I_{12}Z$ phases.

2. Experimental section

The general techniques, including the methods of loading the reactions and running these within welded Ta containers and Guinier powder diffraction with an internal standard on the products, have been described before [10,14]. All manipulations were carried out within N_2- or He-filled gloveboxes.

2.1. Syntheses

Elemental Li (Alfa Aesar, 99.9%) and Os or other Z (Alfa Aesar, 99.95%) were stored in a He-filled glovebox and used as received. The binary iodide LiI (Alfa Aesar, 99%) was dried and sublimed under dynamic vacuum before storage in this glovebox. The rare-earth-metal triiodide LaI_3 was prepared by direct reaction of the elements, purified by vacuum sublimation in contact with only Ta [15], and stored in tightly capped vials in the He-filled glovebox. Iodine (Fisher, 99.8%) for this purpose was used as received. Lanthanum (~99.99%) was obtained from the Ames Laboratory in the form of thin cold-rolled sheets, which were stored within the glovebox, scraped with a scalpel to remove any surface films (oxides or "tarnish"), and cut into small pieces immediately before use. Typically, ~0.25 g of reactants were loaded into Ta tubes that had previously been cleaned, crimped, and welded on one end. Their open ends were then tightly crimped, arc-welded under Ar, and sealed into well-evacuated and baked fused silica jackets before being heated in a furnace. Reactions were generally allowed to take place around 900 °C for 1 week.

Phases were identified and yields were estimated by visual examination of Guinier X-ray powder diffraction patterns (Enraf-Nonius FR-552) of the products and comparisons with calculated patterns. Positions of the indexed diffraction lines of known phases and those of Si (NIST, SRM-640b, added as an internal standard) were used in the calculation of lattice parameters and their standard deviations by least-squares refinements. Reported parameters were refined from X-ray powder patterns composed of at least 90% of an $ALa_6I_{12}Z$-type product (as visually estimated) and with at least 10 indexed diffraction lines that matched. It should be realized that only the overall composition of each sample was known unless a $(Li,La)La_6In_{12}Z$ structure was refined as no fractionation of the products was possible. It also became evident that an excess of the lithium reagent was necessary in order to gain samples close to $LiLa_6I_{12}Z$. The excess LiI (or other) was not identifiable.

The most common impurity observed was LaOI. This phase appeared in almost every pattern, usually in $\leqslant$10% yield, and presumably arose from adventitious water evolved from the fused silica, oxygen in the Ta tubing, and other impurity sources.

Initially, reaction mixtures with stoichiometry $LiLa_6I_{12}Os$ were loaded. A number of samples were also loaded for mixed cations on the isolated site, namely $(Li_xLa_{1-x})La_6I_{12}Os$. The values calculated for the $A2$ contents (below) may of course have been affected by errors in measuring alkali metal reactants, evaporative losses during the welding process (rare), and or stoichiometric deviations caused by formation of LaOI during reaction (which sequesters a portion of the loaded La and I).

2.2. Crystallography

Irregular black crystals were mounted in thin-walled glass capillaries with a small amount of degassed

Apiezon L grease, and Laue photos were taken to determine their suitability. Good crystals were found in the products of reactions with loaded composition $Li_2La_6I_{12}Os$. Diffraction data were collected up to $2\theta = 60^\circ$ at room temperature with graphite-monochromated Mo$K\alpha$ radiation on a Rigaku AFC6R diffractometer. Routine indexing and cell reduction readily gave the *R*-centered hexagonal unit cell. The reflection data were empirically corrected for absorption with the aid of 10 ψ-scans. Systematic absences indicated two possible space groups: $R\bar{3}$ (No. 148) or $R3$ (No. 146). The structure was solved by direct methods [16] and refined in the expected centrosymmetric group $R\bar{3}$.

2.3. Neutron powder diffraction

A 3 cm^3 sample of a loaded composition $Li_3La_6I_{12}Os$ was used for neutron diffraction, which was carried out on the General Purpose Powder Diffractometer (GPPD) of the Intense Pulsed Neutron Source (IPNS) at Argonne National Laboratory. Diffraction patterns were collected at an angle of 145.9° at room temperature with the sample enclosed in a capped cylindrical vanadium container. The resulting data were refined by the Rietveld method [17,18] using GSAS [19].

2.4. ^{7}Li MAS-NMR

A small amount of a $LiLa_6I_{12}Os$ sample was ground and diluted with dry chromatographic Al_2O_3 to total volume of ~1 cm^3 in an N_2-filled glovebox, and this was then loaded into the NMR spinner capsule and tightly capped. The capsule was spun at 4 kHz on a Bruker MSL-300 spectrometer at room temperature while the spectrum was measured. Powdered dry LiCl was used as a reference.

2.5. Physical property measurements

Magnetic susceptibility measurements were performed on a Quantum Design MPMS SQUID magnetometer. Unsieved powdered samples (40–70 mg) were loaded into improved fused silica containers [20] in a He-filled glove box. Magnetizations of the samples at 2 or 5 K were checked as a function of the applied field (0–6 T) to screen for possible magnetic impurities, but none was observed. Magnetic susceptibilities were measured at 1, 3, or 5.5 T between 5 and 400 K. The data were corrected for the susceptibility of the container as well as for the standard diamagnetic core values. The susceptibility of each sample was fitted to a generalized Curie–Weiss equation with an additional temperature-independent (van Vleck) term χ_0.

Bulk electrical resistivities were measured over the temperature range of 100–300 K with an Hewlett-Packard 4342A Q-meter operating at ~34 MHz. The powdered samples were sieved to obtain an average particle diameter of 200 μm (40–60 mg), diluted with dry chromatographic Al_2O_3 (total volume ~1 cm^3) to minimize contact between particles, and this was sealed within an evacuated Pyrex ampoule about 5 cm long. This method generally gives values correct within a factor of two and good temperature dependencies [21,22].

2.6. Void space calculation

The AVOID program (part of the XTEL Program Library from Indiana University Molecular Structure Center) was used to calculate void spaces in the $La_7I_{12}Os$-type structure. Given the appropriate input file of atomic positions and element identities, the program calculates the larger voids in the crystal lattice as well as distances to neighboring atoms. In each iteration, the user fills the previous void with an atom and then the program calculates the next largest void.

3. Results and discussion

3.1. Synthesis and structure

The first problems encountered had to do with demonstrating that attempts to substitute Li for La in the seventh position in $La_7(Z)I_{12}$ to give some version of $Li_xLa_{1-x}La_6ZI_{12}$ were successful and that there was no substitution of more Li in other interstitial sites in the lattice.

Previous refinements of the lattice constants of various $ALa_6I_{12}Os$ phases from Guinier X-ray powder diffraction patterns showed that the sizes of the unit cells reasonably increase as the crystal radius of *A* is increased. The cell volume increase in these originates almost entirely from a lengthening of *c* relative to *a*, as the $La_6I_{12}Z$ clusters move apart in that direction to accommodate the larger cations, the separations of the basal I2 remaining fairly constant. For compounds with A = Na, Ca, Sr and Z = Os, the unit cell volumes were found to increase by about 25–70 $Å^3$ over that for $La_7I_{12}Os$. [12] However, for A = Li, Z = Os, the unit cell volume is indistinguishable from that of the parent $La_7I_{12}Z$, making it impossible to establish the substitution of Li^+ for La^{3+} cations by dimensional shifts in their Guinier patterns alone (Table 1). Furthermore, it can be seen that the unit cell volumes change much less as the relatively large transition metal interstitials *Z* are varied. For the lithium compounds with Z = Ru, Os, Ir, Pt, the volume increases only about 25 $Å^3$, 2470 to 2495 $Å^3$, with most of the increase taking place in *a* (Table 2).

Changes in dimensions with the amount of Li loaded might be expected to be small too, but this analysis

Table 1
Refined unit cell constants for some $Li_xLa_6I_{12}Os$[a,b] compositions

Loaded composition	No. of lines	$a(\sigma)$ (Å)	$c(\sigma)$ (Å)	Volume (σ) (Å^3)
$Li_{0.36}La_6I_{12}Os$[c]	28	16.156(4)	10.992(5)	2485(2)
$Li_{0.71}La_6I_{12}Os$[c]	33	16.146(5)	10.968(4)	2476(2)
$Li_{1.43}La_6I_{12}Os$[c]	14	16.147(5)	10.972(4)	2477(2)
$Li_{2.85}La_6I_{12}Os$[c]	17	16.182(5)	10.996(4)	2494(2)
$Li_3La_6I_{12}Os$[d]	19	16.04(1)	11.132(8)	2480(4)
$Li_{4.28}La_6I_{12}Os$[c]	13	16.15(3)	11.03(4)	2491(13)
$Li_7La_6I_{12}Os$[d]	12	16.153(4)	10.971(4)	2479(2)

[a]Space group $R\bar{3}$ (No.148), $Z = 3$.
[b]Dimensions from least-squares refinements of Guinier X-ray powder diffraction patterns with Si as an internal standard; $\lambda = 1.540598$ Å, 23 °C.
[c]Loaded stoichiometry corrected for $LiI \cdot yH_2O$ content.
[d]Loaded with metallic Li.

Table 2
Refined unit cell constants for some (Li,La)$La_6I_{12}Z$ compounds[a]

Compound	No. of lines	a (A)	c (Å)	Volume (Å^3)
$La_7I_{12}Os$	33	16.146(2)	10.971(3)	2476.9(9)
$LiLa_6I_{12}Ru$[b]	20	16.131(2)	10.960(1)	2469.8(6)
$LiLa_6I_{12}Os$	33	16.146(5)	10.968(4)	2476(2)
$LiLa_6I_{12}Ir$	16	16.172(7)	10.957(9)	2482(3)
$LiLa_6I_{12}Pt$	22	16.187(4)	10.995(4)	2495(2)

[a]As in Table 1.
[b]Loaded compositions were $Li_1La_6I_{12}Z$.

(i.e., of $Li_xLa_6I_{12}Os$ samples, $0<x<1$) was greatly complicated by the discovery that the reactant LiI used initially was, despite previous vacuum sublimation and glovebox storage, contaminated by $LiI \cdot yH_2O$ ($y \leqslant 3$). The stoichiometric parameter x was back-calculated from the amount of contaminated "LiI" loaded in each reaction, assuming that LaOI was the product and the maximum y was 3, although y may not have been constant throughout. Consequently, some subsequent reactions were loaded with metallic Li ($3.0 \leqslant x \leqslant 7.0$), therefore avoiding the impurity problem, and their results compared to those loaded with $LiI \cdot yH_2O$ (with corrected x). The reaction product from loaded composition $Li_3La_6I_{12}Os$ using Li metal did not show any evidence of any other phase in its X-ray powder pattern. The numerical results are presented in Table 2 and shown in Fig. 2. No clear trend of unit cell dimensions with x is indicated. Only three examples gave unit cell volumes more than 3σ different from that of $La_7I_{12}Os$, all three slightly larger than the parent compound, and none had a volume less than that of the parent. Reactions loaded with $\geqslant 4$ equivalents of Li per formula unit showed 15–25% $LiI \cdot yH_2O$ in the powder patterns of the products, while reactions with less did not. Unexpectedly, a small amount of $LiI \cdot yH_2O$ was observed in the products of some reactions loaded with

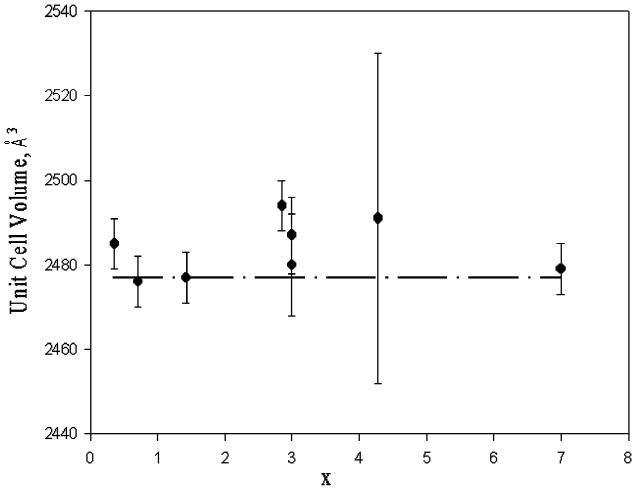

Fig. 2. Unit cell volumes of loaded compositions $Li_xLa_6I_{12}Os$ (circles) and of $La_7I_{12}Os$ (broken line; 2476.9(9) Å^3) (data in Table 1). Bars indicate 3σ error levels.

metallic Li because of contact with traces of moisture. The only other phase observed in these reactions was LaOI (5–10%, if any).

The fact that the lattice constants of $LiLa_6I_{12}Z$ are indistinguishable from those of $La_7I_{12}Z$ (for the same Z) made it very difficult to infer the insertion of Li in the La2 site with certainty (other than the fact that LiI was not an immediate product). However, additional evidence for the incorporation of cations resulted from comparison of the powder diffraction intensities of the 1 0 1 and 1 1 0 reflections, which are the lowest-angle lines in the pattern (near $2\theta = 10°$). For $La_7I_{12}Os$ the 1 1 0 line is calculated to be more intense than the 1 0 1 line, whereas for $LiLa_6I_{12}Os$ the opposite is true. The same pertains when heavier cations (i.e., A = Na, Ca, Sr), substitute for La2 [12]. This of course assumes that other factors, such as preferred orientation within the samples, did not skew the observed intensities. However, the single crystals examined were irregularly shaped, which did not suggest any tendency toward preferred orientation. Table 3 summarizes the results of an assortment of such comparisons that do demonstrate successful substitution of the light cation for La2 in the isolated position. Naturally the calculated pattern of $La_6I_{12}Os$ (with no atom at 0, 0, $\frac{1}{2}$), which is unknown for this rhombohedral $R_7X_{12}Z$ structure, would have intensity ratios that were very similar to those of $LiLa_6I_{12}Os$ (e.g., 1.61 for the Li compound and 1.69 for the hypothetical empty one).

The occupancy problem was quantified by X-ray refinement of a single crystal selected from a high quality product of a sample loaded as $Li_2La_6I_{12}Os$. A summary of some crystallographic parameters is given in Table 4, and the resulting atom positions and anisotropic displacement parameters are listed in Table 5. Important interatomic distances and angles

Table 3
Guinier X-ray powder pattern relative line intensities[a]

Compound[b]		(101)	(110)	(101)/(110)
$La_7I_{12}Os$	Calculated	10.20	28.60	0.36
$La_7I_{12}Os$	Observed	10.01	17.30	0.58
$La_6I_{12}Os$[c]	Calculated	26.90	15.90	1.69
$LiLa_6I_{12}Os$	Calculated	26.40	16.40	1.61
$LiLa_6I_{12}Os$	Observed	15.97	9.98	1.60
$Li_3La_6I_{12}Os$	Observed	33.29	20.00	1.66

[a]Error levels were not included in the intensity output; the data are probably not better than ± 0.01.
[b]Loaded compositions.
[c]Same structure as $La_7I_{12}Os$ but with the La2 position unoccupied.

Table 4
X-ray crystallographic data for $(Li_{0.967}La_{0.033})La_6I_{12}Os$

Space group, Z	$R\bar{3}$ (No. 148), 3
a, c (Å)[a]	16.147(5), 10.972(4)
V (Å^3)	2477(2)
d_{calc} (g/cm^3)	5.122
μ (Mo$K\alpha$, mm^{-1})	22.561
Crystal dimensions (mm)	$0.11 \times 0.10 \times 0.10$
Diffractometer	Rigaku AFC6
Radiation (Å)	Mo$K\alpha$, 0.71069
Scan mode	$2\theta-\omega$
Octants measured, 2θ (max) (deg)	$\pm h$, $+k$, $\pm l$, 60
No. measured reflections	2573
No. independent reflections, R_{int} ($I>0$)	1628, 0.0697
No. independent observed reflections ($I=2\sigma_I$)	766
No. of variables	34
Relative transmission factor range	0.7656–1.0000
Sec. extinction coeff. (10^{-5})	4.5(5)
Goodness of fit	0.950
$R1$, w$R2$ ($I\geqslant 2\sigma_I$)	0.0429, 0.0710
$R1$, w$R2$ (all data)	0.1570, 0.0928
Largest residual peaks (e/Å^3)	1.66 (0.8 Å from I1), −1.91 (0 Å from Os)

[a]Refined cell constants from 14 Guinier lines, $\lambda=1.540562$, 23 °C.

are given in Table 6. Isotropic refinement of the isolated position at 0, 0, $\frac{1}{2}$ as only La gave $R1$, w$R2$ values of 22.1%, 63.8%, respectively, and a U_{eq} value for La2 that was considerably greater than the other atoms' U_{eq}. When this position was refined as 100% Li, its U_{eq} vanished but $R1$ and w$R2$ improved to 9.0%, 27.0%, respectively. The refinement of the Li occupancy (with U_{eq} fixed at the average value of the other atoms) failed to converge, but the constrained anisotropic refinement of the position shared by Li and La2 resulted in $R1$, w$R2$ of 4.3%, 9.3%, with occupancies of 96.7(1)% Li and 3.3(1)% La2. The U_{eq} for Li/La2 was about twice as large as that of the other atoms, but the cavity may be a bit oversized (see below). Since the Li–La2 site in the end members of the series $Li_xLa_{1-x}La_6I_{12}Os$ are evidently fully occupied, we presume all intermediate systems are as well.

Table 6
Important interatomic distances and angles (Å, deg) in $(Li_{0.967}La_{0.033})La_6I_{12}Os$ (Å)

Atoms	d	Atoms	d
Os–La1	2.8743(9)	La1–I1	3.224(1)
Li/La2–I1	3.108(1)	Li/La2–I1	3.228(1)
La1–I2[a]	3.246(1)	La1–La1	4.050(2)
La1–I2[a]	3.250(1)	La1–La1	4.079(2)
La1–I2[b]	3.414(1)	I1–I1[c]	4.316(1)
Atoms	Angle	Atoms	Angle
La1–Os–La1	90.41(3)	Li/La2–I1–La1	89.61(3)
La1–Os–La1	89.59(3)	La1–I1–La1	77.77(4)
I1–Li/La2–I1	180.00(4)	La1–I2–La1	77.79(4)
I1–Li/La2–I1	87.94(3)	La1–I2–La1	173.56(4)
I1–Li/La2–I1	92.06(3)	La1–I2–La1	95.91(4)

[a]Waist bridging I2.
[b]Exo bonded I2.
[c]Shortest I–I contact.

Table 5
X-ray positional and anisotropic displacement parameters for $(Li_{0.967}La_{0.033})La_6I_{12}Os$[a]

Atom	x	y	z	Occ.	B_{eq}	
La1	0.83818(6)	0.15261(8)	0.0230(2)	1	0.0228(2)	
I1	0.96155(8)	0.3245(1)	0.0308(2)	1	0.0292(2)	
I2	0.76503(8)	−0.0019(1)	0.0375(3)	1	0.0206(3)	
Os	0	0	0.0129(3)	1	0.0130(3)	
Li	$\frac{1}{2}$	0	0.05(2)	0.967(1)	0.05(2)	
La2	$\frac{1}{2}$	0	0.05	0.033(1)	0.05	
Atom	U_{11}	U_{22}	U_{33}	U_{23}	U_{13}	U_{12}
La1	0.0228(5)	0.0228(4)	0.0242(4)	–0.0050(4)	–0.0048(4)	0.0117(4)
La1	0.0292(5)	0.0329(5)	0.0270(5)	0.0090(5)	–0.0036(5)	0.0130(4)
I2	0.0206(4)	0.0372(6)	0.0402(7)	0.0130(6)	–0.0078(5)	0.0036(4)
Os	0.0130(4)	U_{11}	0.0129(7)	0	0	$\frac{1}{2}U_{11}$
Li	0.05(2)	U_{11}	0.05(3)	0	0	$\frac{1}{2}U_{11}$
La2	0.05	U_{11}	0.05	0	0	$\frac{1}{2}U_{11}$

[a]Hexagonal setting.

The foregoing efforts do not establish whether Li may also be occupying interstitial sites elsewhere in the lattice. Therefore, the void spaces in the structure of $LiLa_6I_{12}Os$ were calculated using atomic coordinates from the single crystal X-ray refinement, initially with the 0, 0, $\frac{1}{2}$ position empty. The first iteration of the program showed that this position is the most regular and largest available. It has six I1 neighbors, all at 3.11 Å, a reasonable Li–I distance (the sum of crystal radii of six-coordinate Li^+ and I^- is 2.96 Å [23]). A second void is unsymmetrical, with two I1 and two I2 nearest neighbors at 3.12 Å as well as one I1 and one I2 next-nearest neighbors at 3.22 Å. All other voids have four or fewer I neighbors and are smaller, with separations from neighboring iodines less than the sum of crystal radii of four-coordinate Li^+ and I^- (2.79 Å). The six largest voids are summarized in Table 7. If a second Li site exists in this structure, it would most likely be in the second void, but no suitable residual was observed at that position according to X-ray or neutron diffraction. These calculations did not take into account possible effects of the Li cation on positions of the neighboring atoms in the $(Li_{0.967}La_{0.033})La_6I_{12}Os$ structure. There is no lanthanide example of rhombohedral "$R_6X_{12}Z$" (without an atom at 0, 0, $\frac{1}{2}$) available for comparison, although there are zirconium analogues, e.g., $Zr_6Cl_{12}H$ [24].

Fig. 3 shows the neutron powder diffraction pattern at room temperature collected from a composition of $Li_3La_6I_{12}Os$. The refinement began with the symmetry and atomic parameters previously established by single crystal X-ray diffraction in the space group R, with the occupancy of the isolated position set to 100% Li. Isotropic refinement gave unacceptably large U_{iso} for Li (0.40 $Å^2$), about 20 times larger than the average U_{iso} for the other atoms. A fractional La atom was allowed to share the Li position, and the occupancy refined to 57(3)% Li, 43(3)% La2 with $U_{iso} = 0.062(2)$ $Å^2$. Summaries of data collection and isotropic refinement parameters and structural results are given in Tables 8 and 9. An attempted anisotropic refinement was not well-conditioned.

Table 7
Largest calculated void spaces in $LiLa_6I_{12}Os$

Void	x	y	z	Neighbors
1[a]	0	0	$\frac{1}{2}$	6 I at 3.11 Å[b]
2	0.77	0.09	0.50	4 I at 3.12; 2 I at 3.22 Å
3	0.55	0.59	0.42	3 I at 2.69 Å
4	0.10	0.74	0.43	2 I at 2.65; 2 I at 2.82 Å
5	0.15	0.62	0.27	2 I at 2.61; I at 2.69 Å
6	0	0	0.74	3 La1 at 2.60; I at 2.74 Å

[a]The La2 position.
[b]Uncertainty in the distance values are probably ±0.01 Å or less.

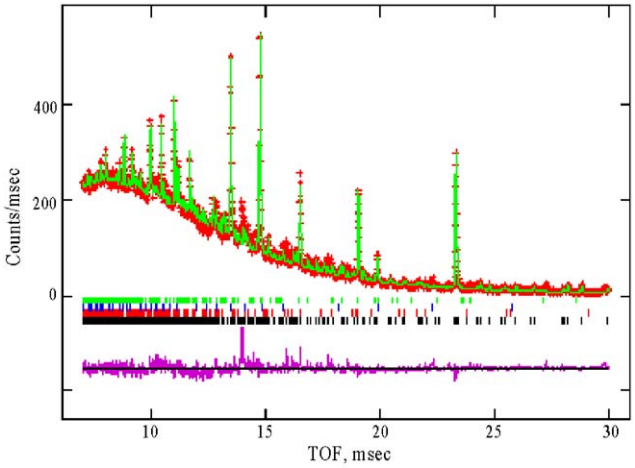

Fig. 3. Neutron powder diffraction pattern at $2\theta = 145.9°$ for the sample refined as $Li_{0.57}La_{0.43}(La_6I_{12}Os)$. In the top portion the black crosses are: observed data, the solid gray line: calculated pattern. Vertical ticks beneath mark the calculated positions of diffraction peaks for: $(Li_{0.57}La_{0.43})La_6I_{12}Os$, LaOI, $LiI\cdots H_2O$, and LaI_3, respectively, and the difference curve is plotted at the bottom.

Some diffraction peaks were not accounted for by the calculated $(Li_{0.57}La_{0.43})La_6I_{12}Os$ pattern, and contamination by impurity phases was suspected. The Guinier X-ray powder pattern taken before neutron diffraction showed ~10% of LaOI ($P4/nmm$) and 5–10% LaI_3 ($P6_3/m$). These two phases were added to the refinement and accounted for some of the less intense diffraction peaks. Although not seen in the X-ray powder pattern, $LiI\cdot yH_2O$ ($Pm3m$) was also observed in the neutron refinement ($\leqslant 5\%$), presumably because of the more efficient scattering of neutrons by these relatively light atoms. About five peaks, the most intense of which was ~100 counts/ms (located at ~14 ms) remained unexplained. The final isotropic R_{wp} and R_p were 8.2% and 5.3%, respectively, while the large reduced χ^2 value was probably a result of the failure to fully account for all of the peaks in the spectrum.

Most of the results of the neutron refinement were consistent with results of X-ray diffraction. Table 10 compares the distances. The isotropic displacement parameters from neutron vs. X-ray refinements are also comparable. Some of the distance differences in Table 10 must arise from the ~40% difference in the lithium vs. lanthanum occupancies. The distances within the structures are consistent with those found in structural analyses of other $A(Li_6X_{12}Z)$ isotypes [11–14]. Subtle effects of the alteration of the A atom are also observed. For example, comparison of the present Li vs. Na [11] results, the closest relative in the group, shows consistent differences. From Li to Na, $d(A$–I1) increases 0.21 Å in comparison with 0.12 Å in Shannon's CN6 crystal radii [23] for the cations. The difference presumably reflects the presence of greater covalent shortening for lithium.

A parallel effect shows in 0.03–0.04 Å increases in d(La1–I1) on the basal faces. All other changes are of the order of ± 0.01 Å except for an increase in the exo-distance La1–I2 of 0.04 Å, which parallels the larger increase in a (0.20 Å) vs. c (0.07 Å) for this change.

3.2. Physical properties

Room temperature ^{7}Li MAS-NMR data from a sample of powdered $LiLa_6I_{12}Os$ showed a single sharp peak centered at -10.22 ppm (vs. solid LiCl) accompanied by a pair of spinning sidebands (Fig. 4). The single resonance confirms a single Li position of high symmetry in the compound, consistent with the single crystal picture in which Li is at the center of a (nearly octahedral) trigonal antiprismatic arrangement of iodine atoms. The absence of any other peaks in the spectrum is further evidence that there are no other competitive sites in the structure significantly occupied by Li.

A previous static ^{7}Li NMR study of cubic $Li_2Zr_6Cl_{15}Mn$ [25], a similar compound made up of Mn-centered Zr_6 clusters surrounded by edge-bridging Cl^{i} atoms and interconnected by $Cl^{a–a}$ bridges showed a triplet spectrum centered at –0.4 ppm (vs. solid LiCl). The Li in the Zr compound has six Cl neighbors arranged nearly octahedrally (D_{2d} symmetry), but the site is only one-third occupied. The greater chemical shift in the Zr compound, as compared to the $LiLa_6I_{12}Os$ sample, is probably the result of decreased shielding because of the more electronegative Cl neighbors.

Bulk resistivities of three powdered compositions were measured by the "Q" method, $La_7I_{12}Os$ and two $Li_xLa_6I_{12}Os$ compositions. All of the samples showed decreasing resistivity with increasing temperature, indicative of semiconducting behavior, as the example in Fig. 5 shows, and room temperature resistivities ranged between 133 and 204 μΩ cm (Table 11). The electrical

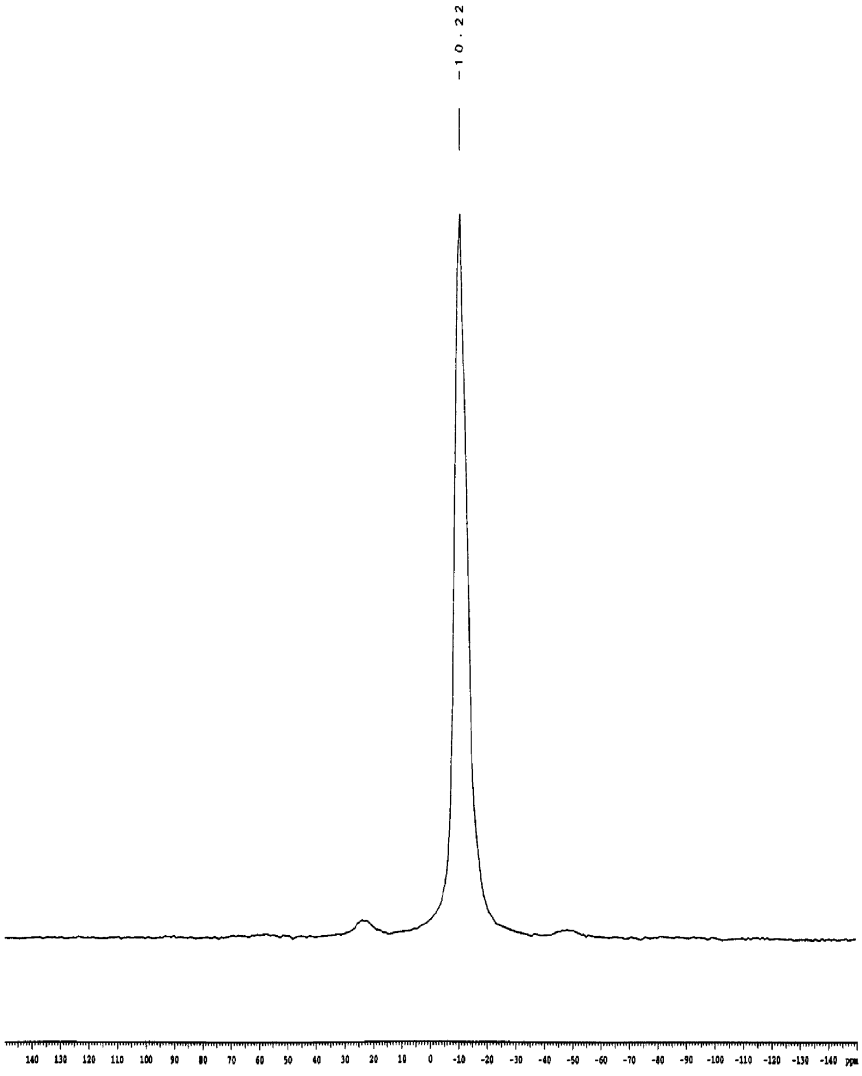

Fig. 4. ^{7}Li NMR of $LiLa_6I_{12}Os$ sample between ± 150 ppm with LiCl(s) as reference. The single peak is centered at -10.22 ppm.

Table 8
Neutron crystallographic data for the powdered sample loaded as $Li_3La_6I_{12}Os$

Space group, Z	$R\bar{3}$, 3
a, c (Å)	16.1709(5), 10.9981(7)
V (Å^3)	2490.7(2)
d_{calc} (g/cm^3)	5.220
Absorption coefficient	0.032752(5)
Diffractometer	IPNS-GPPD
Detector bank, 2θ (deg)	145.9
Histogram scale factor	3.62(2)
R_{wp}, R_p	0.0817, 0.0533
Number of data points	4596
Reduced χ^2	3.053
Diffractometer zero point	−9.09(5)

Refined background and (pseudo-Voigt) profile coefficients.

Background coefficients	Profile coefficients
1 = 0.199(4)	$\alpha = 3(3)$
2 = 0.0052(5)	$\beta_0 = 0.0403(9)$
3 = −0.00026(5)	$\beta_1 = 0.006(1)$
4 = 0.000012(2)	$\gamma_1 = 3.1(6)$
5 = −0.00000027(5)	$\sigma_1 = 109(8)$
	$\sigma_2 = -0.2(10)$

Table 9
Positional parameters for $Li_{0.57}La_{0.43}La_6I_{12}Os$ refined from neutron powder diffraction data[a]

Atom	Fraction	x	y	z	U_{iso} (Å^2)
La1	1	0.8821(5)	0.8376(4)	0.1519(7)	0.0230(9)
Os	1	0	0	0	0.0304(3)
I1	1	0.6155(10)	0.4644(8)	−0.008(1)	0.0241(2)
I2	1	0.6863(8)	0.7630(10)	−0.005(1)	0.0355(2)
Li	0.57(3)	0	0	$\frac{1}{2}$	0.062(2)
La2	0.43(3)	0	0	$\frac{1}{2}$	0.062(2)

[a]Space group $R\bar{3}$ (No.148).

Table 10
Selected interatomic distances in $(Li_xLa_{1-x})La_6I_{12}Os$ structures (Å)[a]

Atoms	Neutron	X-ray	Atoms	Neutron	X-ray
Os–La1 (× 6)	2.884(2)	2.8743(9)	La1–I1	3.245(5)	3.224(1)
Li/La2–I1 (× 6)	3.158(5)	3.108(1)	La1–I1	3.269(5)	3.228(1)
La1–I2[b]	3.262(3)	3.246(1)	La1–La1	4.071(2)	4.050(2)
La1–I2[b]	3.266(3)	3.250(1)	La1–La1	4.085(2)	4.079(2)
La1–I2[c]	3.374(3)	3.414(1)	I1–I2[d]	4.370(2)	4.316(1)

[a]Room temperature data. Different refined occupancies of Li, 0.967 in X-ray sample, 0.57 in neutron diffraction sample, are presumably reflected in the distance differences as well.
[b]Waist bridging I2.
[c]Exo bonded I2.
[d]Shortest I–I contact.

resistivities of most noncondensed ternary and quaternary lanthanide halide cluster compounds have not been reported, but those known have nearly always been

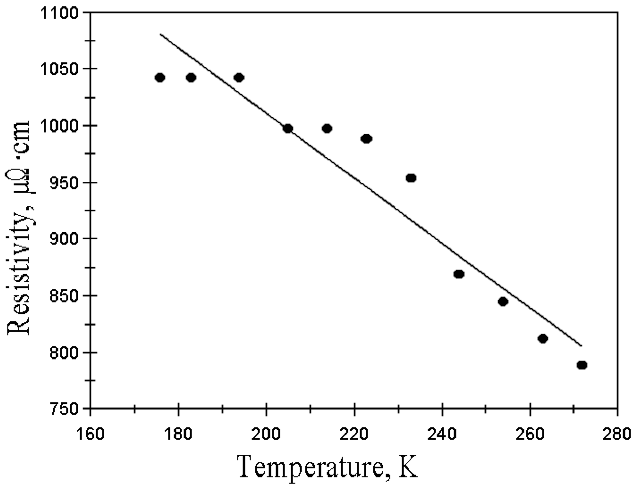

Fig. 5. The electrical resistivity of a sample of $Li_{0.5}La_6I_{12}Os$ by the Q method. The extrapolated resistivity at 298 K is 172 μΩ cm and the mean fractional temperature dependence ($d\rho/dT \cdot \rho$) is $-0.013\,K^{-1}$.

Table 11
Electrical resistivities of $ALa_6I_{12}Z$ compounds by the "Q" method

Loaded composition	$\rho_{298\,K}$ (μΩ cm)[a]
$La_7I_{12}Os$	167, 169, 184
$Li_{0.5}La_6I_{12}Os$	172, 173
$Li_2La_6I_{12}Os$	133, 204

[a]Multiple values correspond to repeat experiments on the same sample.

insulators or poor semiconductors. One example is $La_{12}I_{17}Fe_2$, which contains pairs of iodine-sheathed La_6Fe octahedra in which some of the iodine atoms bridge one edge in each of two adjacent clusters (I^{i-I}) and others have unusual I^{i-a-a} functionality, bridging an edge of one cluster and forming terminal exo-bonds to two other clusters [26]. Its resistivity showed a negative temperature coefficient and an ~350 μΩ cm value at room temperature, though this may have been an underestimate owing to a LaI_2 impurity. In the anomalous metallic α-$K_4R_6I_{14}Os$ (R = La, Pr), the octahedral clusters are interconnected by planar I^{i-a} bridges to form two-dimensional networks. These networks give rise to low and substantially temperature-independent bulk resistivities of ~120–240 μΩ cm, in the range of a poor metal [11]. Given the structure of the present compounds, there seems to be no reason to expect other than semiconducting properties. The metal clusters are linked to adjacent clusters three dimensionally by noncoplanar iodine bridges, and the metal cations are isolated from the clusters as well as from each other by iodine atoms.

Relatively few magnetic susceptibility studies of these cluster halides have been reported, although the simple

MO scheme put forth in early studies [27] suggested relatively simple spin-only results might pertain, the electronic configurations being readily altered via changes in the electron counts of different interstitials. Magnetic susceptibilities were measured for four different $Li_xLa_6I_{12}Os$ compositions at a field strength of either 1 or 3 T and between ~5 and 300 K. Magnetization data as a function of field showed no evidence of ferromagnetic impurities in any of the samples. The susceptibility data for each sample were fitted to a presumed Curie–Weiss equation modified by an additional temperature-independent paramagnetic (van Vleck) term χ_0. The results are collected in Table 12.

Most samples showed small θ values but significant deviations from a Curie–Weiss description, especially at 100–200 K and above, as typified by that shown in Fig. 6. These often quite sharp deviations appear in $1/\chi$ vs. ω plots as regions of different slope and do not seem to depend either on the particular elements or the formal cluster electron counts. Since all of the samples were obtained with high yield (95–100%, estimated by powder X-ray diffraction patterns) of the $ALa_6I_{12}Z$ product, and none showed evidence of ferromagnetic impurities, the possibility of deviations arising from sample contamination seems low. Instead, the observed more complicated susceptibilities presumably arise from correspondingly more complex magnetic structures.

In one explanation, the ground state of the cluster can be described as Curie–Weiss paramagnetic at lower temperatures, but at higher temperatures, or under the influence of the external magnetic field, one or more excited states become electronically populated, resulting in mixtures of ground and excited state(s) paramagnetic characteristics. Spin–orbit coupling between La cluster atoms and the heavy transition metal Z is also a real possibility. To explore this further, the susceptibilities of a sample of the same $Li_2La_6I_{12}Os$ loaded composition was measured at both 1 and 5.5 T. Both measurements showed similar Curie–Weiss behavior at low temperatures with similar magnetic moments (Table 12) and nearly temperature-independent susceptibility at higher temperature, Fig. 7, though neither displayed the abrupt transition that had been observed in others at 3 T. The behavior of the susceptibilities at 5.5 T was less clear above about 100 K, giving an array of widely scattered points (possibly indicating that the sample shifted inside its container), whereas the data for the 1 T measurement continued to fall along a well-defined although nonlinear curve. In addition, none of the effective magnetic moments calculated at lower temperature (Table 12) is

Table 12
Curie–Weiss parameters and calculated effective magnetic moments for $Li_xLa_6I_{12}Os$ products

Loaded composition	Field (T)	Temperature (K)	χ_0, 10^{-4} (emu/mol)	C, (emu K/mol)	θ (K)	μ_{eff} (μ_B)	χ_{300}, 10^{-4} (emu/mol)
$Li_{0.5}La_6I_{12}Os$	3	6–300	5.95(6)	0.0302(6)	−5.1(3)	0.492	7.38(6)
$LiLa_6I_{12}Os$	1	2–350	8.77(4)	0.0270(1)	−2.26(9)	0.465	9.79(4)
$Li_2La_6I_{12}Os$	3	6–300	6.27(2)	0.0146(2)	–4.8(2)	0.342	6.93(2)
$Li_2La_6I_{12}Os$	1	2–350	9.16(5)	0.0128(3)	−2.4(1)	0.320	9.54(5)
$Li_2La_6I_{12}Os$	5.5	2–350	5.91(2)	0.0146(2)	−5.1(1)	0.341	6.34(2)
$Li_3La_6I_{12}Os$	1	2–320	9.8(1)	0.0208(3)	−1.92(7)	0.408	9.7(1)

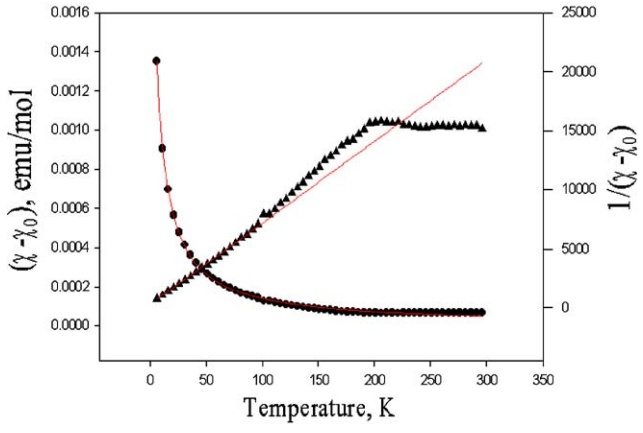

Fig. 6. Magnetic susceptibilities measured at 3 T for a sample loaded as $Li_2La_6I_{12}Os$. Circles and triangles represent χ and $1/\chi$, respectively, each corrected by a van Vleck term (χ_0), and the line marks the best Curie–Weiss fits to all data.

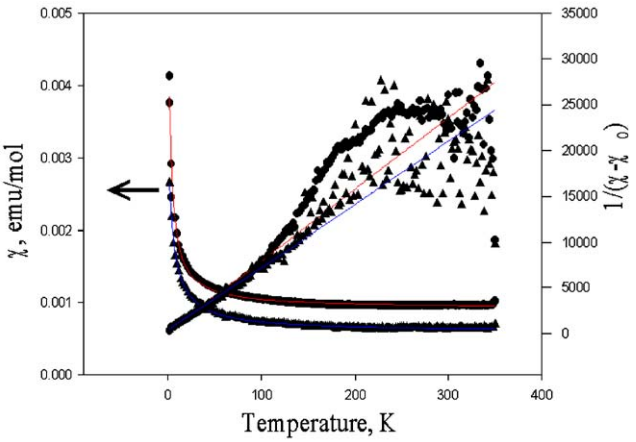

Fig. 7. Magnetic susceptibility of an $Li_2La_6I_{12}Os$ sample at 1 T (circles) and 5.5 T (triangles). Fits to the modified Curie–Weiss equation (right scale) are shown by the straight lines.

consistent with the ideal spin-only values, $\sim 1.7\,\mu_B$ and $\sim 2.9\,\mu_B$ for one and two unpaired electrons, respectively, rather all of the μ_{eff} values fall in the range 0.342–0.492 μ_B. These numbers indicate that a spin-only description is not appropriate for these phases, although some past work involving similar clusters has resulted in seemingly good agreements. Compounds with isolated $(M,R)_6X_{12}$-type clusters that gave μ_{eff} values much closer to the expected spin-only values include $Zr_6I_{12}Mn$ [27] (1.84(7) μ_B), $Sc_6I_{11}C_2$ [28] (1.8(1) μ_B), $Sc_7I_{12}C$ [4] (isostructural with the $ALa_6I_{12}Z$ series, 1.7 μ_B), $CsZr_6I_{14}C$ [29] (1.48 μ_B), $La_{12}I_{17}Fe_2$ [26] (1.11(2) μ_B), and α-$K_4La_6I_{14}Os$ [11] (0.77 μ_B). All of these examples were predicted to have a single unpaired electron per cluster. In addition, $CsLa_6I_{10}Z$ [6] with isolated R_6X_{12} clusters, would have one unpaired electron for $Z = Fe$ and two for $Z = Mn$, consistent with the observed μ_{eff} values of 1.4 and 2.9 μ_B, respectively. None of the above was reported to have deviations in magnetic susceptibility at higher temperatures comparable to those found here except for isostructural $Sc_7I_{12}C$ [4] for which a flattening at ~300 K was postulated to result from "thermal population of neighboring levels".

4. Conclusions

The quaternary lanthanide halide cluster compounds $Li_{1-x}La_6I_{12}Os$ $(0 < x < 1)$ have been synthesized by high-temperature solid-state techniques in the rhombohedral structure type known for many $R(R_6X_{12}Z)$ phases. Single crystals of the compounds were structurally characterized to show that Li occupies the isolated $R2$ position halfway between $R_6I_{12}Z$ clusters along c. The compounds are semiconductors according to isotropic electrical resistivity measurements. However, the magnetic susceptibility data are complex, yielding low μ_{eff} values relative to their ideal formulations and deviations from linearity above ~100 K.

Acknowledgments

The authors thank Jerome Ostenson and Serguei Bud'ko for the magnetic measurements, Chris Murphy and Robert Henning for the neutron diffraction data collection and refinement, and Shu Xu for the NMR measurements. This work was supported by the National Science Foundation—Solid State Chemistry—via Grants DMR-9510278, -9809850, and -0129785, and was carried out in the facilities of the Ames Laboratory, US Department of Energy.

References

[1] A. Simon, H.j. Mattausch, G.J. Miller, W. Bauhofer, R.K. Kremer, in: K.A. Gschneidner, L. Eyring (Eds.), Handbook on the Physics and Chemistry of Rare Earths, vol. 15, Elsevier Science Publishers, Amsterdam, 1991, p. 191.
[2] J.D. Corbett, J. Alloys Compd. 229 (1995) 10.
[3] M. Lulei, J.D. Martin, L.M. Hoistad, J.D. Corbett, J. Am. Chem. Soc. 119 (1997) 513.
[4] D.S. Dudis, J.D. Corbett, S.J. Hwu, Inorg. Chem. 25 (1986) 3434.
[5] T. Hughbanks, J.D. Corbett, Inorg. Chem. 27 (1988) 2022.
[6] M. Lulei, J.D. Corbett, Z. Anorg. Allg. Chem. 622 (1996) 1677.
[7] M. Lulei, J.D. Corbett, Inorg. Chem. 35 (1996) 4084.
[8] M. Lulei, P.A. Maggard, J.D. Corbett, Angew. Chem. Int. Ed. Engl. 35 (1996) 1704.
[9] H.M. Artelt, T. Schleid, G. Meyer, Z. Anorg. Allg. Chem. 618 (1992) 18.
[10] S. Uma, J.D. Corbett, J. Solid State Chem. 161 (2001) 161.
[11] S. Uma, J.D. Martin, J.D. Corbett, Inorg. Chem. 38 (1999) 3825.
[12] E.A. Jensen, J.D. Corbett, Inorg. Chem. 41 (2002) 6199.
[13] E.A. Jensen, J.D. Corbett, J. Solid State Chem. 172 (2003) 132.
[14] E.A. Jensen, J.D. Corbett, J. Solid State Chem. 144 (1999) 175.
[15] J.D. Corbett, Inorg. Synth. 22 (1983) 31.
[16] SHELXTL, Version 5.1; Bruker AXS: Madison, WI, 1998.
[17] H.M. Rietveld, J. Appl. Crystallogr. 2 (1969) 65.
[18] R.A. Young, The Rietveld Method, Oxford University, New York, 1993.
[19] A.C. Larson, R.B. Von Dreele, GSAS: General Structure Analysis System, Low Alamos National Laboratory, Los Alamos, NM, 1986–1994.
[20] A.M. Guloy, J.D. Corbett, Inorg. Chem. 35 (1996) 4669.
[21] J. Shinar, B. Dehner, B.J. Beaudry, D.T. Peterson, Phys. Rev. B 37 (1988) 2066.
[22] J.-T. Zhao, J.D. Corbett, Inorg. Chem. 34 (1995) 378.
[23] R.D. Shannon, Acta Crystallogr. A 32 (1976) 751.
[24] R.P. Ziebarth, J.D. Corbett, J. Solid State Chem. 80 (1989) 56.
[25] J. Zhang, J.D. Corbett, Inorg. Chem. 30 (1991) 431.
[26] M. Lulei, J.D. Martin, J.D. Corbett, J. Solid State Chem. 125 (1996) 249.
[27] T. Hughbanks, G. Rosenthal, J.D. Corbett, J. Am. Chem. Soc. 110 (1988) 1511.
[28] D.S. Dudis, J.D. Corbett, Inorg. Chem. 26 (1987) 1933.
[29] J.D. Smith, J.D. Corbett, J. Am. Chem. Soc. 107 (1985) 5704.